A DETAILED MODELING, ANALYSIS AND SIMULATION OF AN OUT-IN CONFIGURATION VACUUM MEMBRANE DISTILLATION (VMD) PROCESS

Kim Y.-D. and Kim W.-S.*
*Author for correspondence
Department of Mechanical Engineering,
Hanyang University,
Ansan, Gyeonggi-do 15588,
Republic of Korea,
E-mail: wskim@hanyang.ac.kr

ABSTRACT

A detailed rigorous theoretical model has been developed to predict the transmembrane flux of a shell-and-tube type vacuum membrane distillation (VMD) module for seawater desalination. There are primarily two modes of operation to carry out VMD: lumen-side feed (in-out configuration) and shell-side feed (out-in configuration). In this study, detailed mathematical formulations are derived, not for in-out configuration since it has been observed to be restricted by operational constraints such as crystallization in the lumen side of the hollow fiber at high seawater concentrations, but for out-in configuration commonly used in seawater desalination applications. For the out-in configuration VMD module, in spite of the much lower viscosity of water vapor than liquid phase, the pressure build-up of water vapor in the lumen should not be overlooked as the pressure build-up directly reduces the driving force for vapor permeation through the membrane pores. Experimental results and model predictions for mean permeate flux are compared and shown to be in good agreement. The property variation of feed and permeate sides along the axial direction is also examined. Further, the influences of operating parameters (feed temperature and flow rate, hollow-fiber length) on the permeate flux are evaluated, and the pressure build-up of the water vapor in the lumen side is also investigated.

INTRODUCTION

Membrane distillation (MD) is a thermally-driven process which utilizes a hydrophobic, microporous membrane as a contactor to facilitate water vapor separation by liquid-vapor equilibrium. The driving force of MD permeate flux is the partial vapor pressure difference maintained at both interfaces of the membrane, i.e., hot feed and cold permeate. The hot feed is brought into contact with the membrane which allows only the vapor to pass through its dry pores so that it condenses on the coolant side [1,2].

Several MD module configurations have been proposed, e.g. direct contact membrane distillation (DCMD), air gap membrane distillation (AGMD), sweeping gas membrane distillation (SGMD) and vacuum membrane distillation (VMD). More recently, other new MD configurations aiming to enhance the permeate flux have been developed, such as liquid gap MD (LGMD) and material gap MD (MGMD) [1,2]. Among them, VMD is regarded to possess a great potential for scale-up as it offers the highest flux and efficient heat recovery compared to the other configurations [1], though that AGMD may provide similar of better internal heat recovery as condensation takes place inside the module. However, in the VMD process the condensation of water vapor takes place outside the module using a vacuum pump, which is regarded as the main drawback of this configuration compared to others, e.g. AGMD. AGMD has also several disadvantages such as complex module design and low permeate flux.

In VMD process, the hollow-fiber membranes have been widely implemented due to their high membrane packing densities leading to high membrane surface area, and as a result its module has been shown to be advantageous over plate-and frame and spiral modules for seawater desalination applications. The hollow-fiber MD module has mainly two operating modes, e.g. lumen-side feed (in-out configuration) and shell-side feed (out-in configuration). Both feed configurations have been extensively studied for VMD process, and each mode has its own advantages and potential problems. However, the lumen-side feed configuration has been observed to be restricted by operational constraint, especially due to crystallization in the fiber lumen at high seawater concentrations, and fouling and scaling problems. In this regard, shell-side feed configuration has been commonly used in seawater desalination applications. For the out-in configuration module, however, despite much lower viscosity of the water vapor compared to the liquid phase, the pressure build-up of vapor in the fiber lumen should not be disregarded as the pressure build-up promptly deteriorates the driving force for vapor permeation through the membrane. Especially, this is very important in module design for practical applications. However, this aspect has not been addressed in details in previous literatures [3,4,5].

The main objectives of present work are thus (i) to develop a detailed mathematical model for the shell-and-tube type VMD with the shell-side feed configuration for seawater desalination, by simplifying the mass, momentum and energy balance on both the feed and permeate sides, (ii) to evaluate the influences of operating parameters such as feed temperature, flow rate and hollow-fiber length on the permeate flux and thus (iii) to examine the pressure build-up characteristics of water vapor in the fiber lumen.

HOLLOW FIBER VMD PROCESS

Figure 1 illustrates a schematic of a hollow-fiber VMD module with two different flow configurations, i.e., parallel (top) and counter (bottom). The hollow-fiber VMD module comprises an array of microporous hydrophobic membranes, assembled together in a shell-and-tube module. As shown in Figure 1, the hot feed is circulated in contact with the shell side of the hollow fiber and the permeate is evolved in the vapor state from the opposite side of the membrane which is kept under low pressure (vacuum). One end of the fiber lumen is open to provide an outlet for the evacuation of water vapor from the module, and vacuum is applied to the open end of the fiber. Therefore, the vapor pressure in the fiber lumen increases from the open end to the opposite end, which results in a pressure build-up along the fiber lumen leading to a decrease in the driving force ($P_{f,m} - P_p$). This phenomena will be examined in details in what follows to elucidate the effects of pressure build-up in the fiber lumen on the VMD permeate flux.

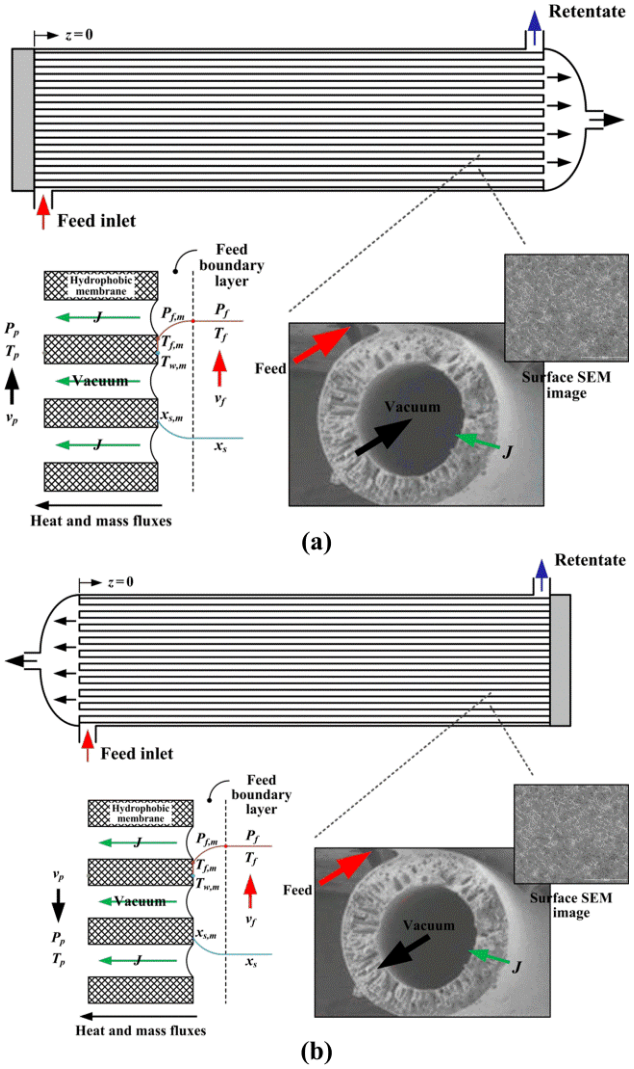

Figure 1 Schematic representation of hollow-fiber VMD module with an out-in configuration in (a) parallel- and (b) counter-flow configurations

MATHEMATICAL MODEL

Transmembrane Flux

VMD process involves the heat transfer across the feed-side boundary layer adjacent to the membrane surface and through the membrane, coupled with the mass transfer of water vapor through a membrane. The heat transfer process entails the heat transferred across the feed-side boundary layer (Q_f) and through the membrane (Q_m). Here, the heat transfer by conduction through the membrane and across the permeate-side boundary layer can be assumed to be negligible [3,4,5].

The convective heat transfer (Q_f) across the feed-side boundary layer is defined as follows:

$$Q_f = h_{tf}\left(2\pi r_o N_f\right)\left(T_f - T_{f,m}\right) \tag{1}$$

where h_{tf}, r_o, N_f, T_f and $T_{f,m}$ are the convective heat transfer coefficient, the outer radius of fiber, the number of hollow fibers, the bulk feed temperature and liquid/vapor interface temperature at the feed side, respectively. The convective heat transfer coefficient (h_f) at the shell side is determined by the Groehn's correlation [6]:

$$Nu = \frac{h_{tf} d_h}{k_f} = 0.206\left(\mathrm{Re}\cos\alpha\right)^{0.63}\mathrm{Pr}^{0.36} \tag{2}$$

where k_f is the heat conductivity of the bulk feed and α is the yaw angle varying between 0° for the cross flow and 90° for the parallel flow. d_h is the hydraulic diameter of the shell, $d_h = d_o\left(1-\phi\right)/\phi$, which is a function of the module packing density ϕ, $\phi = N_f\left(d_o/d_s\right)^2$, with denoting d_s the shell inner diameter.

The heat transfer across the membrane can be expressed by the latent heat of vaporization. The heat transfer through the membrane can be determined as:

$$Q_m = J\left(\pi N_f d_{lm}\right)\left[h_v\left(T_{f,m}\right) - h_f\left(T_f\right)\right] \tag{3}$$

with $d_{lm} = \left(d_o/d_i\right)/\ln\left(d_o/d_i\right)$, where h_v and h_f refer to the specific saturated enthalpies of water vapor and bulk feed, respectively, which are evaluated at the local temperatures, i.e., $T_{f,m}$ and T_f.

The overall heat transfer across the membrane at steady state is given by:

$$Q_f = Q_m \tag{4}$$

The permeate flux of the water vapor (J_z) is linearly related to its partial pressure gradient as follows:

$$J_z = K_m\sqrt{M}\left(P_{f,m} - P_p\right) \tag{5}$$

where K_m is the permeability coefficient, M is the molecular weight of water, $P_{f,m}$ is the water vapor pressure at the liquid/vapor interface at the feed side and P_p is the pressure at the permeate side. Due to the presence of dissolved species with molar concentration (x_s) at the feed side, the vapor pressure reduction can be determined by the Raoult's law by assuming seawater as an ideal solution for simplicity:

$$P_{f,m} = \left(1 - x_s\right) P_{w,m} \tag{6}$$

where $P_{w,m}$ is the pure water vapor pressure (in Pa) and estimated using the Antoine equation [7]:

$$\log_{10}\left(133.3 P_{w,m}\right) = 8.07131 - \frac{1730.63}{T + 233.426} \tag{7}$$

where T is the temperature in ºC.

In the VMD process, the molecule-molecule collisions are negligible as compared to the molecule-pore wall collisions as the membrane pores are considerably smaller than the mean free path of the diffusing molecules. In this way, the Knudsen diffusion mechanism controls the mass transfer through the membrane pores. Thus, the permeability coefficient can be estimated as:

$$K_m = \frac{4\varepsilon d_p}{3\tau\delta\left(2\pi RT\right)^{1/2}} \tag{8}$$

where ε is the fractional void volume of the membrane, d_p is the pore size, τ is the pore tortuosity, δ is the membrane thickness and R is the universal gas constant.

Transport Models

To demonstrate the transport behavior in the hollow-fiber module, a mathematical model is formulated by using mass, momentum and energy balances for both feed and permeate sides with following assumptions: (i) unidirectional lubrication flow of Newtonian fluid for the shell-side feed, (ii) steady incompressible flow under constant operating conditions, (iii) fibers distributed uniformly in the shell side, (iv) negligible heat generation due to viscous dissipation, (v) ideal gas behavior of water vapor in the permeate side, (vi) negligible heat loss to the ambient and (vii) negligible axial diffusion compared to convection.

The mass (i.e., overall molar balance and molar species balance for the salt species), momentum and energy balances for the feed flow in the shell side yield the following equations, (9)–(12), in terms of velocity (v_f), concentration (x_s), pressure (P_f) and temperature (T_f):

$$\frac{1}{X_f}\frac{dv_f}{dz} - \frac{v_f}{{X_f}^2}\left(\frac{M_s}{\rho_s} - \frac{M_w}{\rho_w}\right)\frac{dx_s}{dz} = -\frac{2r_o N_f J}{M_f\left(r_s^2 - N_f {r_o}^2\right)} \tag{9}$$

$$\frac{x_s}{X_f}\frac{dv_f}{dz} + \frac{v_f}{{X_f}^2}\frac{M_w}{\rho_w}\frac{dx_s}{dz} = 0 \tag{10}$$

$$\frac{d}{dz}\left(\rho_f v_f^2\right) + \frac{2\rho_f v_f^2 f}{D_h} + \frac{dP_f}{dz} = 0 \tag{11}$$

$$\rho_f v_f \frac{d}{dz}\left(c_{p,f} T_f\right) - \frac{v_f}{{X_f}^2}\frac{2r_o N_f J}{r_s^2 - N_f {r_o}^2} c_{p,f} T_f = -\frac{2\pi r_o N_f h_{tf}\left(T_{f,b} - T_{f,m}\right)}{\pi\left(r_s^2 - N_f {r_o}^2\right)} \tag{12}$$

where X is the molar volume, z is the local axial coordinate, ρ is the density, r_o is the outer radius of hollow fiber, r_s is the inner radius of shell, μ is the dynamic viscosity, c_p is the specific heat capacity and subscripts s, w and f are the salt, water and feed phases, respectively. The dimensionless quantity f defined in equation (11) refers to the fanning friction factor and $f = 16/\mathrm{Re}$ in the laminar-flow regime. For the turbulent flows, the fanning friction factor can be estimated using the Wood's approximation based on the Colebrook equation [8]:

$$f = a + b\,\mathrm{Re}^{-c} \tag{13}$$

with

$$a = 0.0235\left(\frac{\varepsilon}{d_h}\right)^{0.225} + 0.1325\left(\frac{\varepsilon}{d_h}\right)$$
$$b = 22\left(\frac{\varepsilon}{d_h}\right)^{0.44} \tag{14}$$
$$c = 1.62\left(\frac{\varepsilon}{d_h}\right)^{0.134}$$

where ε is the membrane surface roughness.

The mass, momentum, energy balances for the permeate flow in the fiber lumen provide coupled differential equations, (15)–(17), in terms of velocity (v_p), pressure (P_p) and temperature (T_p):

$$v_p T_p \frac{dP_p}{dz} + P_p T_p \frac{dv_p}{dz} - P_p v_p \frac{dT_p}{dz} = \frac{2r_o R {T_p}^2 J}{M_v r_i^2} \tag{15}$$

$$\left(M_v {v_p}^2 + RT_p\right)\frac{dP_p}{dz} + 2M_v P_p v_p \frac{dv_p}{dz} - \frac{M_v P_p {v_p}^2}{T_p}\frac{dT_p}{dz} = -\frac{M_v P_p {v_p}^2 f}{r_i} \tag{16}$$

$$\frac{P_p v_p}{T_p}\frac{dh_v(T_p)}{dz} + \frac{2r_o RJ}{M_v r_i^2}\left[h_v(T_p) - h_v(T_{f,m})\right] = 0 \tag{17}$$

where f in equation (16) is the fanning friction factor for the fully developed laminar flow in a circular tube.

Boundary Conditions

The velocity, concentration, pressure and temperature at the shell side for both parallel- and counter-flow configurations are subject to the following boundary conditions:

$$v_f(0) = v_{f,in},\ x_f(0) = x_{f,in},\ P_f(L_f) = P_0,\ T_f(0) = T_{f,in} \tag{18}$$

where L_f is the fiber length, P_0 is the ambient atmospheric pressure at the feed outlet and subscript *in* is the module inlet.

The velocity, pressure and temperature at the permeate side for parallel- and counter-flow configurations are subject to the following boundary conditions:

$$v_p(0) = 0,\ P_p(L_f) = P_{vac},\ T_p(0) = T_{f,m}(0) \tag{19}$$

$$v_p(L_f) = 0,\ P_p(0) = P_{vac},\ T_p(L_f) = T_{f,m}(L_f) \tag{20}$$

where P_{vac} is the vapor pressure (vacuum) applied to the open end of the VMD module.

In order to calculate the performance of a VMD module, the mean permeate flux (J_m) of a VMD module is determined as:

$$J_m = \frac{1}{L_f}\int_0^{L_f} J_z dz \tag{21}$$

where J_z is the local permeate flux defined in equation (5).

Solution Procedure

The set of coupled ordinary differential equations (ODEs) for the shell-side feed, i.e., equations (9)–(12), and for the lumen-side permeate, i.e., equations (15)–(17), are discretized with the finite volume method and solved by coupling the boundary conditions, i.e., equations (18)–(20), and the membrane characterizations, i.e., equations (1), (3) and (4) for heat transfer and equations (5)–(8) for mass transfer. Broyden's method, which is the quasi-Newtonian method for solving the system of nonlinear equations, has been implemented. The detailed solving procedure is discussed in [3] in details. Thermophysical properties of water and seawater used in the present work are implemented from [9].

RESULTS AND DISCUSSION

In this study, two mathematical models are applied to clarify the effect of pressure build-up of water vapor in the fiber lumen on VMD performance; that is, (i) simple lumped model (SM) in which the permeate-side pressure is kept constant over the entire length of the hollow-fiber membrane without considering only the permeate-side transport equations (15)-(17) and (ii) detailed model (DM) taking into account of pressure build-up in the fiber lumen by considering all of the governing equations aforementioned.

Spatial Variation

In order to verify and further examine the proposed theoretical approaches, the performance characteristics of shell-and-tube VMD module, as previously reported [10], have been examined with respect to feed temperature and velocity at the inlet of the VMD module. The primary characteritics of a polypropylene (PP) hollow-fiber membrane module are: shell diameter: 0.025 m; number of fibers: 40; mean pore size: 0.2 μm; inner fiber diameter: 1.8 mm; outer fiber diameter: 2.6 mm; effective membrane area: 0.1 m^2; liquid entry pressure (LEP): 140 kPa, porosity: 70%; fiber length: 0.47 m. The permeate-side vacuum pressure is kept constant at 4 kPa and the pure water is used in the experiments [10].

As illustrated in Figure 2, using two theoretical models (i.e., SM and DM), the predicted mean permeate fluxes as a function of feed velocity in the range of 0.2 m/s – 1.0 m/s and feed temperature in the range of 35 °C – 60 °C are compared to the measured data [10]. For the operating conditions ($T_{f,in}$ = 50 °C, $v_{f,in}$ = 0.4 m/s) in Figure 2, the axial variations of permeate flux, pressure, temperature and velocity along the fiber length using two models for parallel- and counter-flow configurations are

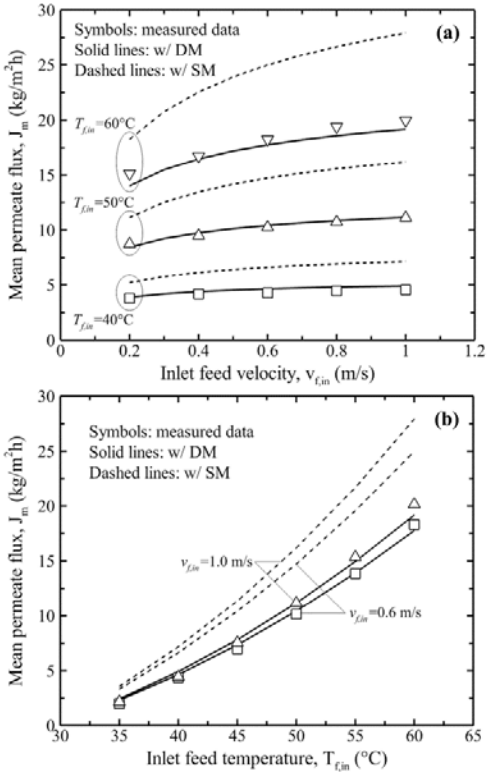

Figure 2 Mean permeate flux as a function of (a) feed velocity for the different feed temperatures and (b) feed temperature for the different feed velocities using SM and DM models.

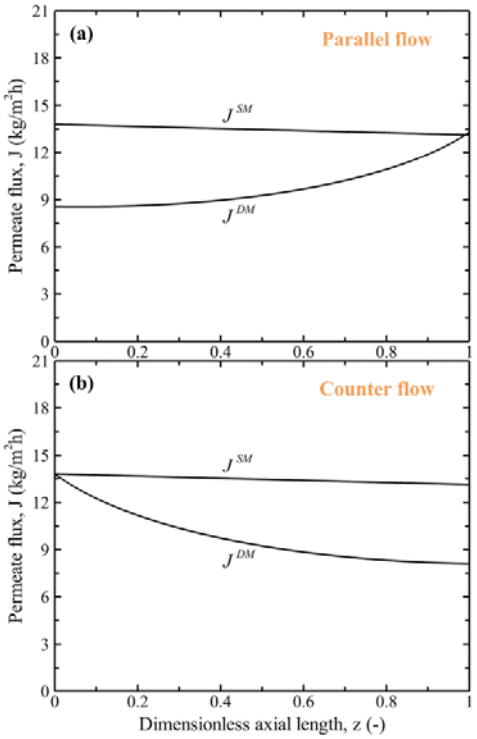

Figure 3 Comparison of permeate flux profiles along the hollow fiber using SM and DM models: (a) parallel- and (b) counter-flow configurations.

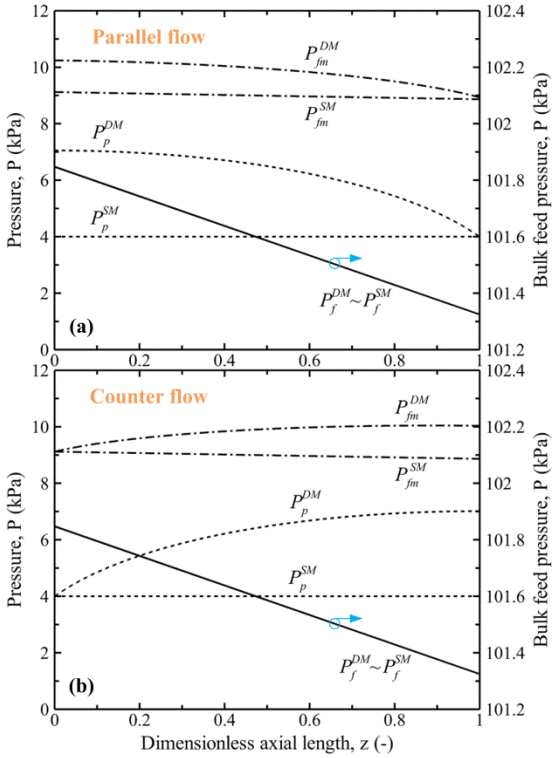

Figure 4 Comparison of pressure profiles along the hollow fiber using SM and DM models: (a) parallel- and (b) counter-flow configurations.

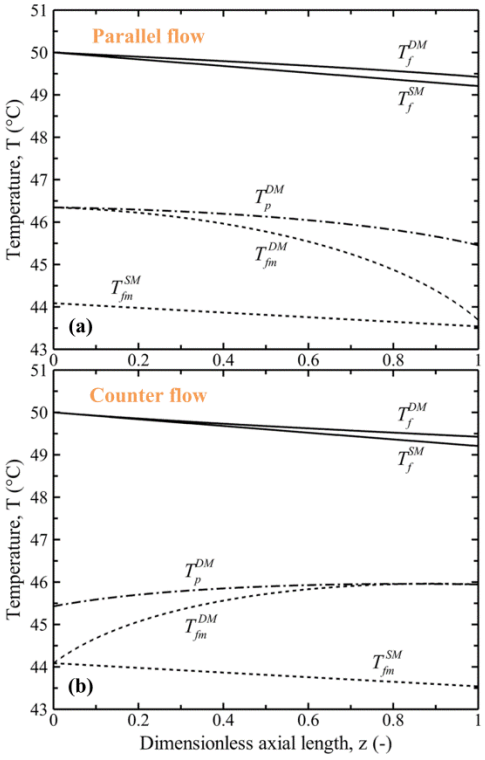

Figure 5 Comparison of temperature profiles along the hollow fiber using SM and DM models: (a) parallel- and (b) counter-flow configurations.

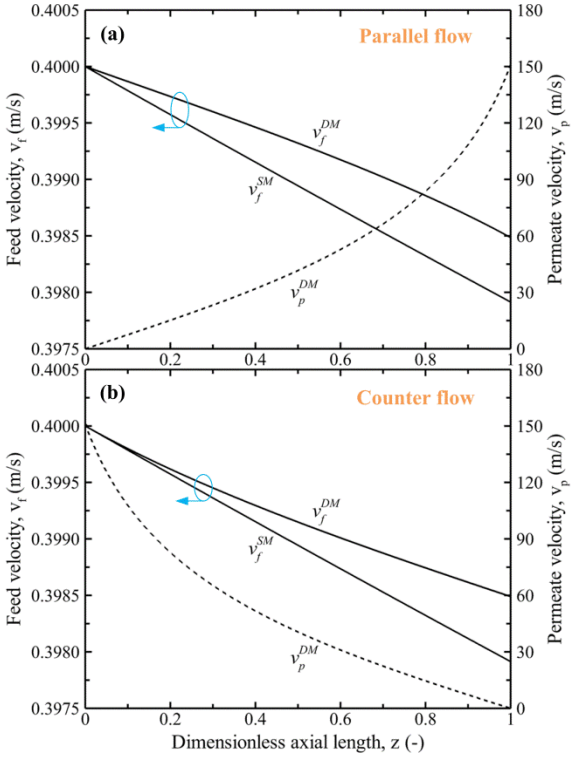

Figure 6 Comparison of velocity profiles along the hollow fiber using SM and DM models: (a) parallel- and (b) counter-flow configurations.

depicted in Figures 3–6, respectively. It can be seen that there is a significant pressure build-up of water vapor in the fiber lumen. As seen from Figure 2, therefore, it is found that while the SM model with keeping permeate pressure constant is easy to use, it tends to highly overestimate by about 30% – 46% the mean permeate flux as compared to that of the DM model. It can also be observed that an increase in feed temperature will result in a more significant pressure build-up. This may be explained as follows: As can be expected from Figures 3–6, the permeate flow rate increases as the vapor flows along the fiber length from the dead end of the fiber to the open end, and it reaches maximum at the open end of the fiber. At a higher temperature, the saturation vapor pressure increases exponentially, and so does the driving force for vapor permeation, leading to a higher permeate flux. On the other hand, there will be a large pressure change where the permeate flow rate is high.

As shown in Figure 2, it is shown that the permeate flux enhances with an increase in the inlet feed velocity and feed temperature. The relative effect of the feed velocity on the permeate flux increases with the temperature, which can be attributed to the combined effects of exponential relationship between temperature and saturation vapor pressure shown in equation (7) and higher heat transfer through the feed-side boundary layer at higher feed velocity (i.e., higher Reynolds number in equation (2)), which results in lower temperature polarization leading to greater transmembrane temperature difference [11]. On the other hand, the feed velocity at lower feed temperatures below 50 °C, resulting in a decrease in the vapor-pressure driving force, can be assumed to have negligible

Table 1 Effects of fiber length and feed velocity on the mean permeate flux using SM and DM models.

L_f [m]	$v_{f,in}$ = 0.05 m/s			$v_{f,in}$ = 0.1 m/s			$v_{f,in}$ = 0.2 m/s		
	J_m [kg/m^{2}h]		(SM–DM)/DM	J_m [kg/m^{2}h]		(SM–DM)/DM	J_m [kg/m^{2}h]		(SM–DM)/DM
	DM	SM	[%]	DM	SM	[%]	DM	SM	[%]
0.1	7.09	7.17	1.22	9.13	9.27	1.57	11.29	11.51	1.95
0.3	6.28	6.89	9.59	8.04	9.03	12.23	9.83	11.32	15.07
0.5	5.40	6.61	22.57	6.83	8.79	28.72	8.22	11.12	35.23
0.7	4.62	6.36	37.70	5.78	8.56	48.09	6.77	10.93	61.59

effects on the permeate flux. Meanwhile, it is noted that the mean permeate flux predicted using the DM model exhibits good agreement with measured data.

Effect of L_f and $V_{f,in}$ on Permeate Pressure Build-up

The effect of the fiber length and feed velocity on the mean permeate flux of the hollow-fiber VMD module with parallel-flow configuration has been demonstrated at the inlet feed temperature of 50 °C by keeping other operating parameters constant as before.

As can be seen in Table 1, the influence of fiber length on the permeate pressure build-up is much greater than that of feed velocity. This is because with an increase in the fiber length the local transfer resistance increases greatly due to the rapid build-up of thermal boundary layers, which reduces the temperature difference through the membrane and thus hinders the mass and heat transfer. In addition, the reduction of mean permeate flux can be found to be attributed to the extremely low temperature gradient across the membrane due to the longer retention time of the feed stream with an increase in the fiber length. Also, the longer fiber length can also result in more nonuniform local flux profile because the longer fiber can lead to the greater pressure drop per unit fiber length caused by larger flow resistance, which causes a higher pressure build-up along the fiber lumen. Meanwhile, the permeate flux can be enhanced by increasing the feed flow rate, which results in improving the hydrodynamic conditions in terms of Reynolds number, heat and mass transfer coefficients. Therefore, it is important to identify the fiber length to assure that the driving force along the fiber is sufficient to maintain a high performance, even though a longer fiber length and yet a larger membrane area can contribute to more water production.

CONCLUSIONS

In the present work, a detailed rigorous theoretical model to predict the transmembrane flux of an out-in configuration VMD module has been developed. Experimental results and model predictions for mean permeate flux are compared and shown to be in good agreement. It is found that while the simple VMD model with keeping permeate pressure constant is easy to use, it is likely to significantly overestimate the mean permeate flux as compared to that of the detailed model taking into account of pressure build-up in the fiber lumen. The pressure build-up of water vapor in the fiber lumen is identified to be the crucial factor significantly influencing the VMD performance since it directly reduces the driving force for vapor permeation through the membrane pores. In addition, its effect is more pronounced at longer fiber lengths and higher permeate fluxes, which can be achieved at higher feed temperatures and velocities. In conclusion, this is especially important in module design for practical applications of VMD processes.

ACKNOWLEDGEMENTS

This research was supported by a grant (code 17IFIP-B065893-05) from Industrial Facilities & Infrastructure Research Program funded by Ministry of Land, Infrastructure and Transport of Korean government and the Korea Institute of Energy Technology Evaluation and Planning (KETEP) and the Ministry of Trade, Industry & Energy (MOTIE) of the Republic of Korea (No. 20153010130460).

REFERENCES

[1] Khayet, M., Membranes and theoretical modeling of membrane distillation: A review, *Advances in Colloid Interface Science*, Vol. 164, 2011, pp. 56-88.

[2] Alkhudhiri, A., Darwish, N., and Hilal, N., Membrane distillation: A comprehensive review, *Desalination*, Vol. 287, 2012, pp. 2-18.

[3] Kim, Y.-D., Thu, K., Ng, K.C., Amy G.L., and Ghaffour, N., A novel integrated thermal-/membrane-based solar energy-driven hybrid desalination system: Concept description and simulation results, *Water Research*, Vol. 100, 2016, pp. 7-19.

[4] Kim, Y.-D., Thu, K., and Choi, S.-H., Solar-assisted multi-stage vacuum membrane distillation system with heat recovery unit, *Desalination*, Vol. 367, 2015, pp. 161-171.

[5] Lee, J.-G., Kim, Y.-D., Shim, S.-M., Im, B.-G., and Kim, W.-S., Numerical study of a hybrid multi-stage vacuum membrane distillation and pressure-retarded osmosis system, *Desalination*, Vol. 363, 2015, pp. 82-91.

[6] Groehn, H.G., Influence of the yaw angle on heat transfer and pressure drop of tube bundle heat exchangers, *Heat Transfer*, Vol. 6, 1982, pp. 203-209.

[7] Felder, R.M., and Rousseau, R.W., *Elementary Principles of Chemical Processes*, John Wiley & Sons, New York, 2000.

[8] de Nevers, N., *Fluid Mechanics for Chemical Engineers*, McGraw-Hill, New York, 1991.

[9] Sharqawy, M.H., Lienhard V, J.H., and Zubair, S.M., Thermophysical properties of seawater: A review of existing correlations and data, *Desalination and Water Treatment*, Vol. 16, 2010, pp. 354-380.

[10] Mengual, J.I., Khayet, M., and Godino, M.P., Heat and mass transfer in vacuum membrane distillation, *International Journal of Heat and Mass Transfer*, Vol. 47, 2004, pp. 865-875.

[11] Kim, Y.-D., Thu, K., Ghaffour, N., and Ng, K.C., Performance investigation of a solar-assisted direct contact membrane distillation system, *Journal of Membrane Science*, Vol. 427, 2013, pp. 345-364.